2D Layered Materials: From Materials Properties to Device Applications

Peida Zhao, Sujay Desai, Mahmut Tosun, Tania Roy, Hui Fang, Angada Sachid, Matin Amani, Chenming Hu, Ali Javey*

Electrical Engineering and Computer Sciences, University of California, Berkeley, CA 94720; Tel: (510) 643-7203,
*Email: ajavey@berkeley.edu

Abstract

An overview of material properties and the current state of electronic devices based on 2D layered materials is presented. Atomic scale smoothness, varying band alignment and sizeable bandgaps in the single layer limit make this class of materials very interesting for optoelectronic applications. Scaling effects, doping techniques, contacts and strain engineering of 2D materials are discussed. In addition, important advancements in 2D material electronic devices, for example the all-2D field effect transistor (FET), heterojunction devices, and tunnel diode are highlighted.

I. Introduction

An ever-growing interest in the various layered 2D materials has led to an extensive investigation of their optical, material, and electronic properties and their application towards devices. Layered 2D materials consist of covalent/ionic in-plane bonding with van der Waals (vdW) interlayer interactions. A large number of 2D layered materials are semiconductors with varying bandgaps and electron affinities. Some examples are transition metal dichalcogenides (TMDs) (e.g. MoS_2, WSe_2), other layered dichalcogenides (e.g. SnS_2, $SnSe_2$), and black phosphorus (BP) as shown in Fig.1 [1-5]. This band alignment variation along with vdW interlayer coupling allows for versatility in designing optimal strain free and atomically sharp heterostructures for diodes, transistors and tunneling devices. Notably, given their layered structure, monolayers with atomic scale smoothness and no dangling bonds can be obtained (although native defects exist practically), thus reducing the effect of surface roughness scattering. A double-gated MOS (DGMOS) structure with a layered semiconductor channel is shown in Fig. 2(a). As shown in Fig. 2(b), the characteristic length and short channel effects in 2D materials are significantly less compared to Si, due to their lower in-plane dielectric constants ($\varepsilon_r \sim 4$ for MoS_2, SnS_2; $\varepsilon_r \sim 9$ for BP) [9]. From the viewpoint of device scaling, this is a major advantage of 2D semiconductors. Lastly, high effective mass (m*) along the channel means that the direct source to drain leakage will also be lower for sub-5nm channel length 2D devices as compared to traditional Si-based FETs [10-13].

II. Material Properties

A. Doping

Fig. 3 highlights the four major approaches taken towards TMD doping, including surface charge transfer [16], covalent functionalization [15], fixed charge layer deposition for remote charge doping [14], and substitutional doping [17]. Each approach presents its own pros/cons for a given TMD in terms of maximum doping concentration, reliability, stability and ease of processing. Table 1 collates the quantitative results for the various doping schemes presented in literature.

B. Contact Engineering

Fig. 4(a) underlines the challenge associated with obtaining ohmic contacts to TMDs, specifically due to Fermi level pinning at the metal/contact interface [18]. The use of ultra-high (ultra-low) work function metal contacts together with heavy doping is needed for low contact resistance for holes (electrons). In this regard, exploring non elemental metals with extreme work functions is advantageous. One example is MoO_x ($x < 3$) [19], a high work function (Φ) material (Φ up to 6.6eV) used to contact the valence band of MoS_2. p-type conduction achieved using MoO_x is comparable to the n-type characteristics obtained with Pd contacts as seen in Fig. 4(c).

C. Strain

Strain can be used to engineer the electronic bandstructure and optoelectronic properties of TMD materials [20-21]. An interesting case is that of WSe_2 multilayers, which undergo an indirect to direct bandgap transition under uniaxial tensile strain [20], similar to Ge as shown in Fig. 5(a-c). This enables application of multilayer TMDs in optoelectronic device applications like photodiodes, solar cells, LEDs, etc. Also a change in bandstructure would lead to a change in the carrier mobility, enabling mobility engineering via strain [22].

III. Device Characteristics

A. MOSFETs

Fig. 6(a) shows a top-gated WSe_2 MOSFET fabricated with doped source/drain (S/D) extensions which decrease the series contact resistance, and enable exploration of the intrinsic material performance. Fig. 6(b) and (c) show the transfer characteristics of WSe_2 MOSFETs incorporating S/D extension doping using surface charge transfer from NO_2 and K, achieving high performance WSe_2 p-FETs (subthreshold swing ~ 60mV/dec and hole mobility ~250 cm^2/Vs) [23] and n-FETs (electron mobility ~110 cm^2/Vs) [24] respectively. Moreover, using the aforementioned techniques, WSe_2 p-FET (using Pt contacts) and n-FET (using S/D extension K doping) are fabricated on the same flake as shown in Fig. 6(d) [25], forming a WSe_2 CMOS

inverter with output and voltage transfer curves shown in Fig. 6(e-f) respectively.

B. All 2D FET

Fig. 7 shows the schematic and device characteristics of an all-2D FET, a new device platform using MoS_2 as channel, graphene as source, drain and gate electrodes and h-BN as the gate dielectric [26]. This device operates as an n-FET with $I_{ON}/I_{OFF} \sim 10^6$. The mobility of MoS_2 is extracted to be ~33 cm^2/Vs after correcting for the contact resistance. Notably, the mobility of the channel does not degrade at high gate electric fields, suggesting the absence of surface roughness scattering. This experimental observation demonstrates a key advantage of layered materials like TMDs over conventional semiconductors especially as scaling progresses towards ultrathin body devices.

C. Heterostructures

Atomically smooth heterostructures with strain free interfaces and sharp band edges are made possible because of the unique properties of layered materials like TMDs [27]. Fig. 8(b) shows the transmission electron microscope (TEM) image of a WSe_2/MoS_2 hetero-bilayer. Due to vdW interlayer bonding, the heterostructure exhibits no structural stress and displays a pristine Moiré pattern arising from the difference in lattice constant and angular orientation. Photoluminescence and absorption measurements as shown in Fig. 8(c) indicate a spatially direct absorption but spatially indirect emission mechanism which is explained in Fig. 8(d). The strong intensity of the spatially indirect emission indicates significant charge coupling across the vdW gap of these heterostructures.

D. TMD Tunnel FET

TMD heterostructures can be configured as tunnel FETs, taking advantage of the theoretically sharp band edges of these layered semiconductors [27]. Fig. 9 shows the operation of a four terminal gate-tunable WSe_2/MoS_2 vdW heterojunction diode [28]. In the dual-gated structure as shown in Fig. 9(a), the bottom and top gates can exert independent electrostatic control over the MoS_2 and WSe_2 layers respectively. In this configuration, the two gates can modulate the band offset and the doping concentrations of WSe_2 and MoS_2 layers thereby tuning the operation of the diode. As the band offset is increased, the diode performance is tuned from a p/n diode to a Zener diode and at the p+/n+ condition to an Esaki diode as shown in Fig. 9(c) and (d).

Moving forward, investigation of material systems with appropriate band alignments and carrier effective mass values, interface engineering, and doping contacts to reduce parasitic resistances are required to achieve high performance TFETs based on heterostructure TMDs.

IV. Outlook

2D layered materials and their interesting properties as highlighted here place them at an important position with respect to traditional semiconductors like Si, Ge and III-V materials. Looking forward, significant work still needs to be done on the high quality growth of these materials over large area. Growth of heterostructures is necessary for achieving clean interfaces essential for improving performance of devices like TFETs. Contact resistance and stable doping techniques are other areas which require significant work to enable greater application of these exciting materials, and realize their potential in solving many future challenges such as device scaling and 3D integration.

References

[1] C. Gong, et. al., Appl. Phys. Lett., 103, 053513, 2013
[2] Y. Cai, et. al., Sci. Rep, 4, 6677, 2014
[3] Y. Xu, et. al., Am. Mineral., 85, p.543, 2000
[4] F. A. Rasmussen, et. al., J. Phys. Chem. C, 119(23), p.13169, 2015
[5] http://www.ioffe.ru
[6] H. Asahina, et. al., J. Phys. C: Solid State Phys., 17 p.1839, 1984
[7] E. J. G. Santos, et. al., ACS Nano, 7(12), p.10741, 2013
[8] Y. Huang, et. al., ACS Nano, 8(10), p.10743, 2014
[9] K. Suzuki, et. al., IEEE Trans. Elec. Dev., 40(*12),* 1993
[10] W. Cao, et. al., IEEE IEDM, p. 729, 2014
[11] V. Mishra, et. al., IEEE IEDM, p. 136, 2013
[12] L. Liu, et. al. IEEE Trans. Elec. Dev., 60(12), 2013
[13] Y. Yoon, et. al., Nano Lett. 11, p.3768, 2011
[14] K. Chen, et. al., Appl. Phys. Lett. Mat., 2(092504), 2014
[15] P. Zhao, et. al., ACS Nano, 8(1), p. 10808, 2014
[16] D. Kiriya, et. al., J. Am. Chem. Soc., 136(31), p.11188, 2014
[17] J. Suh, et. al., Nano Lett., 14, p.6976, 2014
[18] S. Das, et. al., Nano Lett., 13, p. 199, 2013
[19] S. Chuang, et. al., Nano Lett., 14(3), p.1337, 2014
[20] S. B. Desai, et. al., Nano Lett. 14(8), p.4592, 2014
[21] H. J. Conley et. al., Nano Lett. 13(8), p.3626, 2013
[22] J. Welser et. al., IEEE IEDM, p. 373, 1994
[23] H. Fang et. al., Nano Lett., 12 (7), p.3788, 2012
[24] H. Fang et. al., Nano Lett., 13, p.1991, 2013
[25] M. Tosun et. al., ACS Nano, 8(5), p.4948, 2014
[26] T. Roy et. al., ACS Nano, 8(6), p.6259, 2014
[27] H. Fang et. al., PNAS, 110(29), p.11688, 2013
[28] T. Roy et. al., ACS Nano, 9(2), 2071, 2015
[29] M. S. Choi et. al., ACS Nano, 8(9) p.9332, 2014
[30] L. Yang et. al., Nano Lett., 14, p.6275, 2014
[31] D-H. Kang, et. al., ACS Nano., 9(2), p.1099, 2015
[32] A. Rai, et. al., Nano Lett., 15, p.4329, 2015
[33] D. Xiang, et. al., Nat. Commun., 6, 7485, 2015
[34] D. Kiriya, et. al., Adv. Mater., *in press*, 2015

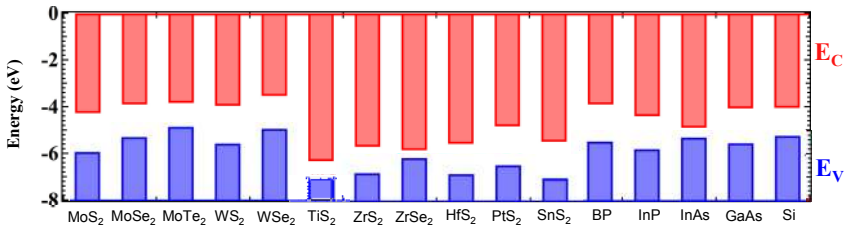

Fig 1. Band alignments of monolayer semiconducting dichalcogenides and monolayer black phosphorus (simulations) compared to selected III-Vs and Silicon. [1-5]

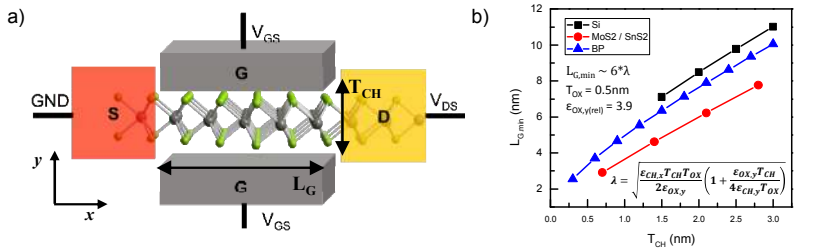

Fig 2. a) Dual-gated MOS (DGMOS) FET with layered semiconductor channel b) Characteristic length and scaling limit reflected via $L_{G,min}$ vs. channel thickness (T_{CH}) for some representative materials. Blue curve: Black Phosphorus T_{CH} = (0.3*N) nm with $\varepsilon_r \sim 9$. Red curve: MoS_2 / SnS_2 = (0.7*N) nm with $\varepsilon_r \sim 4$. Here N is the number of layers. Black curve: Silicon, $T_{CH,\,min}$ =1.5 nm with $\varepsilon_r \sim 12$. [6-9]

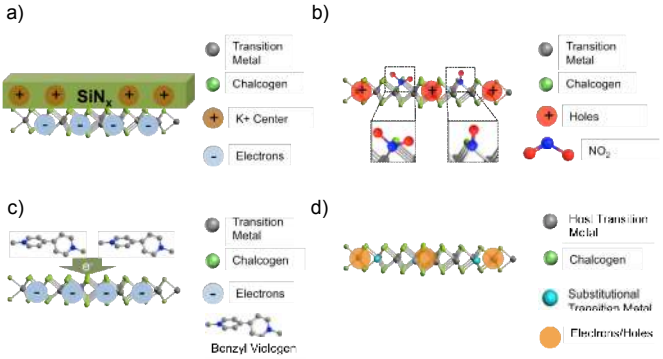

Fig 3. Various TMD doping schemes using specific examples. a) SiN_x as the fixed charge layer. b) Functionalization using NO_2 c) Molecular physisorption of benzyl viologen d) Transition metal substitutional doping. [14-17]

Dopant Species	Polarity on TMD	Max Sheet Concentration (cm^{-2})	Contact Resistance ($k\Omega*\mu m$)	Ambient Stability
Surface Charge Transfer				
NO_2 [23]	WSe_2 (p)	2.2×10^{12}	NA	NA
K [24]	WSe_2 (n) MoS_2 (n)	MoS_2: 2.5×10^{12} WSe_2: 1.0×10^{13}	NA	NA
Benzyl Viologen [16]	MoS_2 (n)	1.2×10^{13}	1.1	≥ 9 days
$AuCl_3$ [29, 34]	MoS_2 (p)	3×10^{13}	NA	NA
Chloride [30]	WS_2 (n) MoS_2 (n)	MoS_2: 9.2×10^{12} WS_2: 6.0×10^{11}	MoS_2: 0.3 WS_2: 0.4	≥ 4 weeks
Cs_2CO_3 (n) MoO_3 (p) [33]	BP (n) BP (p)	1.5×10^{12} (n) 6×10^{12} (p) V_{BG} = +/-30V	5.1×10^{-3} (n) 2.6×10^{-2} (p)	NA
TiO_x [32]	MoS_2 (n)	7.4×10^{12}	NA	Stable
Covalent Functionalization				
NO_x [15]	WSe_2 (p)	1.3×10^{13}	2.54	≥ 2 days
Octadecyltrichlorosilane [31]	WSe_2 (p)	5.2×10^{11}	NA	≥ 3 days
Substitutional Doping				
Nb [17]	MoS_2 (p)	2.8×10^{14}	NA	≥ 1 week
Remote Charge Doping				
SiN_x [14]	WSe_2 (n)	9.5×10^{13}	NA	≥ 2 weeks

Table 1. Summary of major doping schemes reported in literature. The doping methods are classified overall as surface charge transfer, covalent functionalization, substitutional doping, and remote charge doping. [14-17, 23-24, 29-34]

Fig 4. TMD Contact Engineering. a) Fermi level pinning at the MoS_2 Schottky barrier. Adapted with permission from ref 18. Copyright 2013 American Chemical Society. b) Using MoO_x as a high work function metal oxide p-type contact. c) I_DV_G of MoS_2 FETs with Pd (n-FET) and MoO_x/Pd (p-FET) S/D contacts. Adapted with permission from ref 19. Copyright 2014 American Chemical Society.

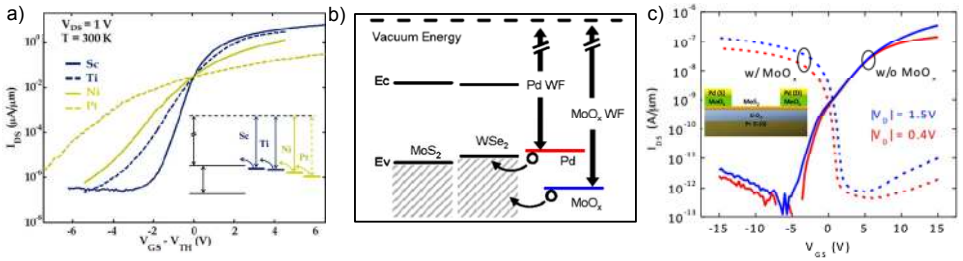

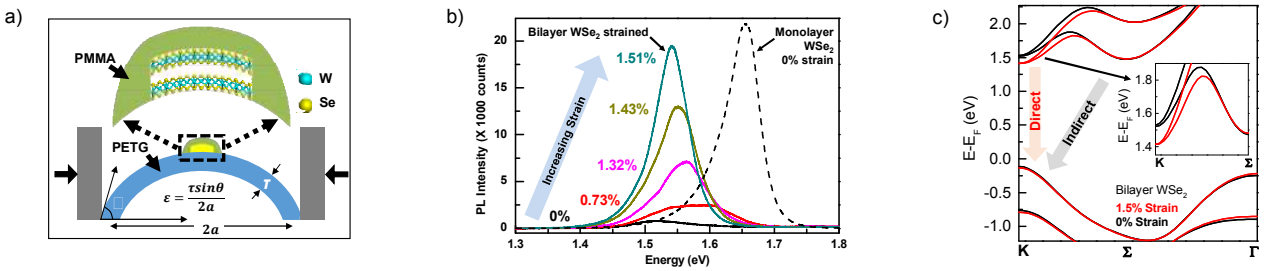

Fig 5. a) Schematic of the 2-point bending apparatus for uniaxial tensile strain. WSe_2 encapsulated by PMMA is transferred onto PETG. τ is the thickness of the PETG, ε is the strain, θ is the tangent angle at the min. strain point and 2a is the separation of the bent PETG. b) Bilayer WSe_2 photoluminescence (PL) spectra at different strain. PL of unstrained monolayer WSe_2 is shown for comparison. c) Electronic band structure for bilayer WSe_2 with and without strain using HSE-DFT. Adapted with permission from ref 20. Copyright 2014 American Chemical Society.

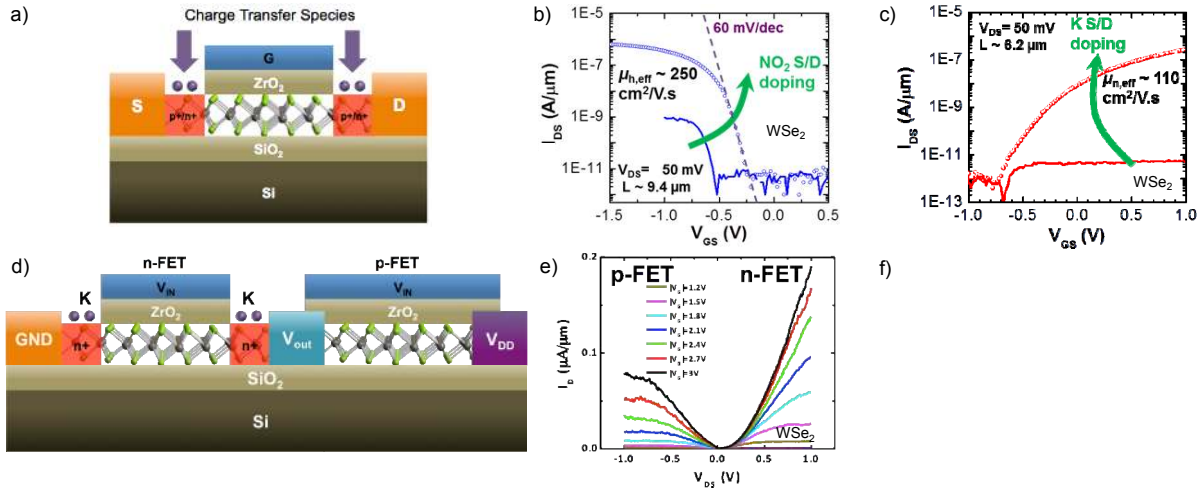

Fig 6. a) General schematic of a top-gated TMD MOSFET with degenerately doped source/drain (S/D) contacts. Here the top-gate acts as the mask to protect the active channel from dopant species. b) Transfer characteristics of a monolayer WSe_2 device with L ~9.4μm before and after NO_2 S/D contact doping [23] c) Transfer characteristics of a 3 layer WSe_2 MOSFET before and after K contact doping [24] d) Schematic of a WSe_2 CMOS inverter. e) Output characteristics of a WSe_2 p-FET and n-FET fabricated on the same WSe_2 flake. f) Voltage transfer characteristics of a WSe_2 CMOS inverter at different supply voltages [25]. Adapted with permission. Copyright 2013 American Chemical Society.

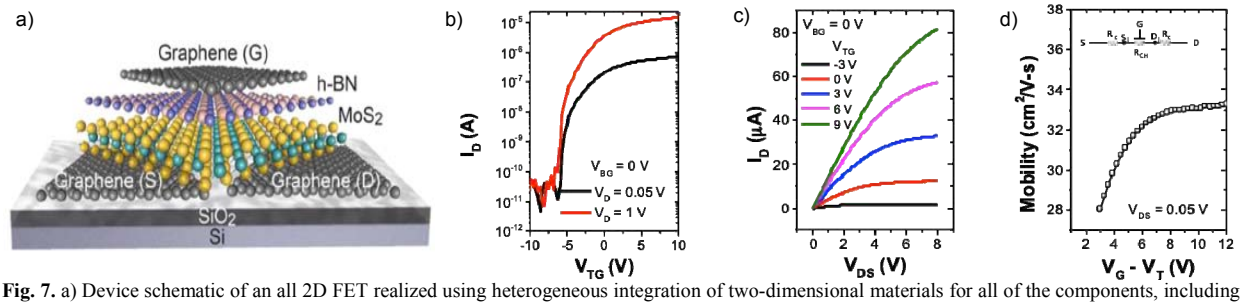

Fig. 7. a) Device schematic of an all 2D FET realized using heterogeneous integration of two-dimensional materials for all of the components, including the channel, gate dielectric and contact layers. [26] b) I_DV_G characteristics at different V_D (c) I_DV_D characteristics. (d) Extracted field effective mobility as a function of gate overdrive, V_G-V_T. The inset shows the circuit model of the device used for mobility extraction. Note that mobility does not degrade as a function of surface scattering at large gate overdrive voltages. The Si substrate is grounded during all measurements.

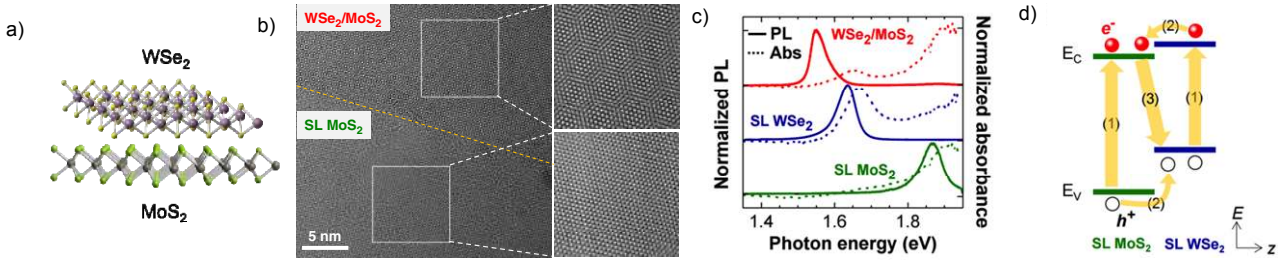

Figure 8. a) Schematic of a WSe_2/MoS_2 hetero-bilayer. [27] b) Transmission emission microscopy (TEM) of a WSe_2/MoS_2 hetero-bilayer, note that a clear Moiré pattern is seen at the hetero-bilayer. c) Normalized photoluminescence (solid lines) and absorbance (dashed lines) spectra of single-layer WSe_2, MoS_2, and the corresponding heterostructure. d) Band diagram of WSe_2/MoS_2 heterostructure under photo excitation, depicting (1) absorption and exciton generation in WSe_2 and MoS_2 single layers, (2) relaxation of excitons at the MoS_2/WSe_2 interface driven by the band offset, and (3) radiative recombination of spatially indirect excitons.

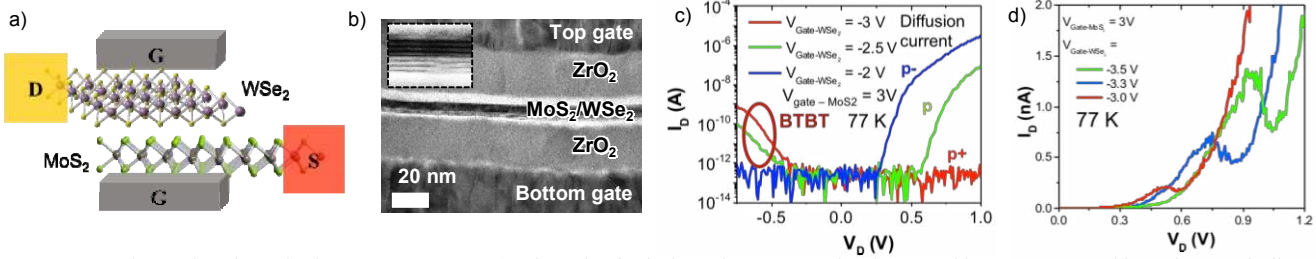

Fig 9. Tunnel-FETs based on vdW heterostructures. [28] a) Schematic of a dual-gated TFET, note that the top and bottom gates are able to electrostatically control the band alignment of the top and bottom TMD layers respectively, allowing for effective band offset modulation at the hetero-interface. b) TEM cross sectional image of a fabricated device, note that MoS_2 and WSe_2 are 4 layers each in thickness for this device. c) Gate tunability of a dual-gated MoS_2/WSe_2 device at 77 K. d) I_DV_D at $V_{Gate\text{-}MoS2}$ = 3 V and $V_{Gate\text{-}WSe2}$ varied. Negative differential resistance is observed at forward bias. Adapted with permission from ref 28. Copyright 2013 American Chemical Society.